Comparision of Band Structures for Fourteen Semiconductors

Akash Malemath, Université de Bourgogne

January 24, 2024

***Abstract*—This report examines and reproduces the pseudopotential formfactors and electronic band structures for 14 semiconductors of the diamond and zincblend structures: AISb, CdTe, GaAs, GaP, GaSb, Ge, InAs, InP, InSb, Si, Sn, ZnS, ZnSe, and ZnTe. The study employs one of the empirical pseudopotential method, renowned for its accuracy and efficiency in crystalline solid state physics discussed in the paper by Cohen and Bergstresser[1] in 1966. The Brillouin zone paths are mapped to ensure a thorough exploration of the electronic states along the specified directions. This paper aims to compute, compare and analyze the bandstructures thereby validating the method used.**

I. Introduction

The goal of this investigation is to calculate the electron band structure for 14 semiconductors enlisted in Table 3.2 of the lecture notes. The computation employs exploring the Brillouin zone path, as defined by the BZpath function from 'BZpath.m' file in Exercise 3.8.6 of the lecture notes. To ensure accuracy, the obtained results will be cross-verified with the findings in the paper by M.L. Cohen and T. K. Bergstresser, titled 'Band Structures and Pseudopotential Form Factors for Fourteen Semiconductors of the Diamond and Zincblende Structures'[1]. The emphasis is on achieving precision comparable to experimental observations, with a minimalistic discussion in line with the original approach. The following sections delve into the form factor determination, pseudopotential Hamiltonian, and present and compare the reproduced results.

II. Theory

The computational procedure initiates by defining the reciprocal unit lattice vectors. Further, this enables the construction of the three dimensional reciprocal space, of size defined by 'cutoff' value, by constructing reciprocal lattice vectors 'G'. The BZpath function from the BZpath file assists us in obtaining the 'qpath'. This is the path in the brillouin zone along which the electronic bandstructure has to be constructed.

Moving onto defining the potential V for each semiconductor, this process involves expanding V in terms of the reciprocal lattice vectors G and incorporating the pseudopotential form factors $V_{|G|^2}$.

$$V_{|G|^2} = cos(G \cdot s)V^s_{|G|^2} + isin(G \cdot s)V^A_{|G|^2} \quad (1)$$

where s and -s = $\frac{a}{8}(1,1,1)$ are the positions of the two atoms relatively to the centre of the primitive cell that is chosen as origin, with a being the length of unit cube. The Table 1 from Cohen and Bergstresser's study[1] is used to calculate the above defined form factors. One important point to note is that, this study omits the $V_{G=0}$ term, taken care in further section in order that the zero of the energy scale is set to the top of the valence band.

The pseudopotential Hamiltonian governing the electronic bandstructure in the defined crystal comprises of both kinetic energy component and a spatially dependent weak potential,

$$H = -(\hbar^2/2m)\nabla^2 + V(\mathbf{r}) \quad (2)$$

The potential V can be Fourier-expanded as defined before in terms of pseudopotential form factor V_G,

$$V(\mathbf{r}) = \sum_G V_G e^{-iG\cdot\mathbf{r}} \quad (3)$$

Further, the hamiltonian matrix comprising of all V_G terms and kinetic energy terms is built adhering to the procedures outlined in the original paper [1] and in the lecture notes of chapter 3 (sections 3.1 to 3.3). The bandstructures are then derived for 14 materials, by diagonalizing the Hamiltonian for defined 16 electronic bands.

III. Results

A thorough comparison has been conducted between the reconstructed band structures as depicted in the subsequent figures, and the original findings from Cohen and Bergstresser's study[1]. The figures showcase close resemblance between the reproduced and the established findings in terms of of the bands constructed and also the curvature of conductance and valence bands, affirming the accuracy of the computational approach. This meticulous analysis confirms the consistency and reliability of the replicated electron band structures for the 14 semiconductors with diamond and zinc-blende structures. Figures 1-28 provide a comprehensive comparison between the electron band structures of various semiconductors.

The band gaps depicted in my plots align closely with those reported by Cohen and Bergstresser, exhibiting minor discrepancies in certain bands. Across all semiconductors, the band gaps demonstrate accurate

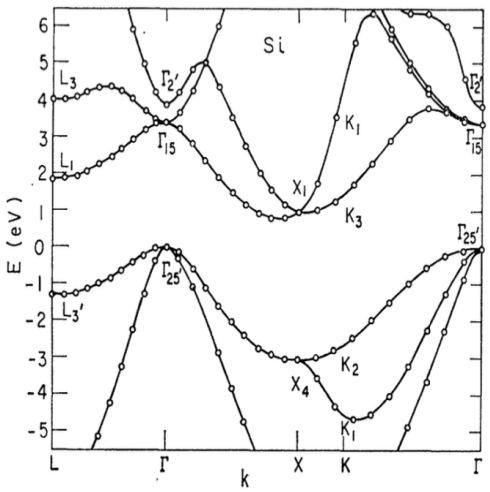

Fig. 1: Band Structure of Si. Cohen,Bergstresser.

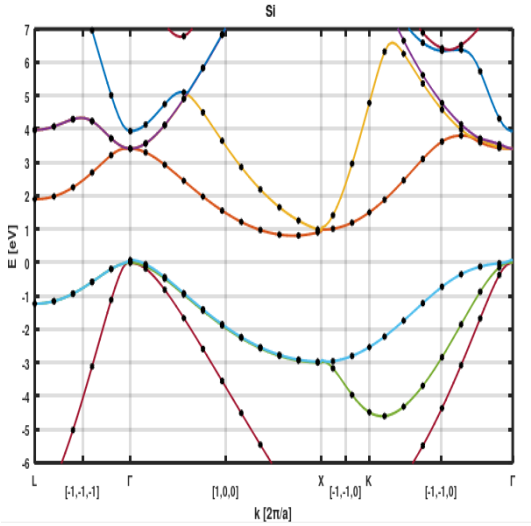

Fig. 2: Reproduced Band Structure of Si

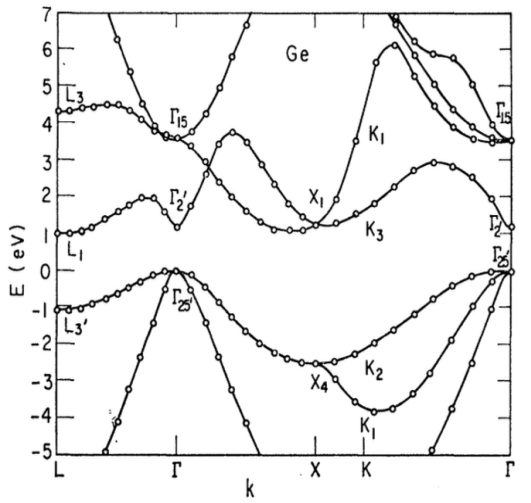

Fig. 3: Band Structure of Ge. Cohen,Bergstresser.

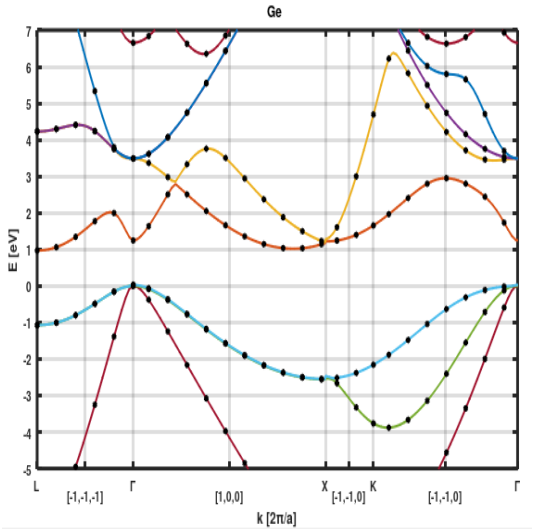

Fig. 4: Reproduced Band Structure of Ge

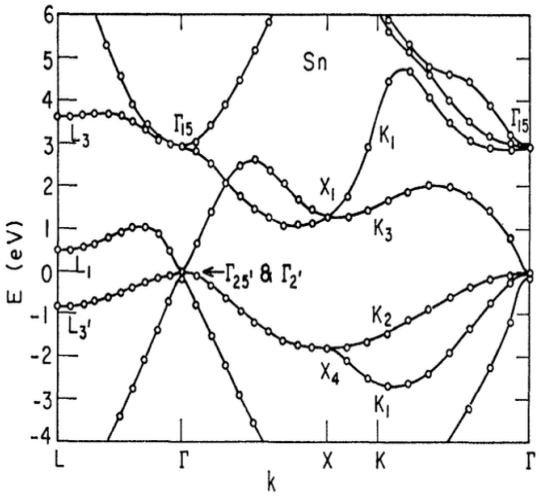

Fig. 5: Band Structure of Sn. Cohen,Bergstresser.

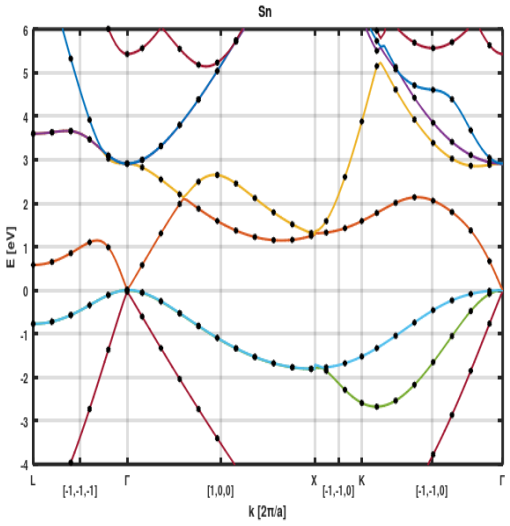

Fig. 6: Reproduced Band Structure of Sn

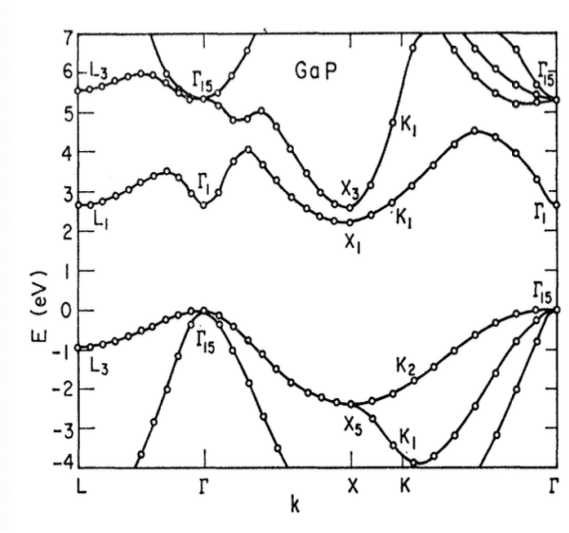

Fig. 7: Band Structure of GaP. Cohen,Bergstresser.

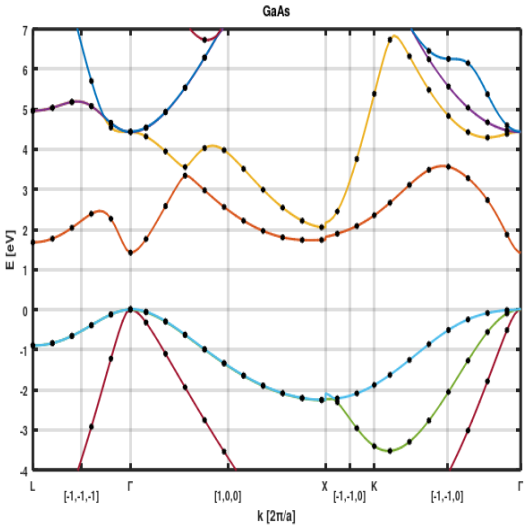

Fig. 10: Reproduced Band Structure of GaAs

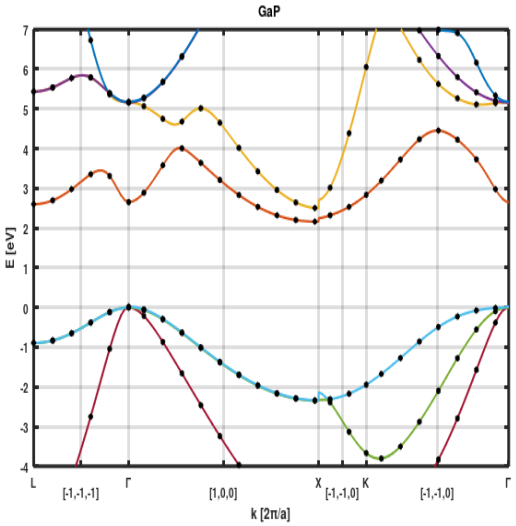

Fig. 8: Reproduced Band Structure of GaP

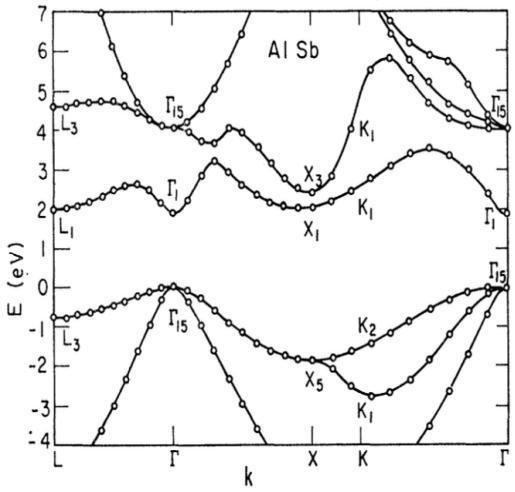

Fig. 11: Band Structure of AlSb. Cohen,Bergstresser.

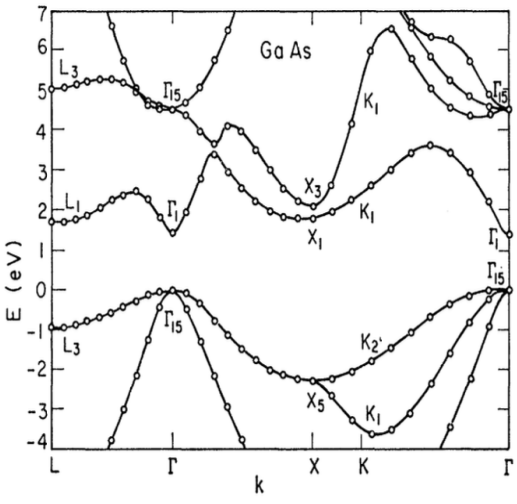

Fig. 9: Band Structure of GaAs. Cohen,Bergstresser.

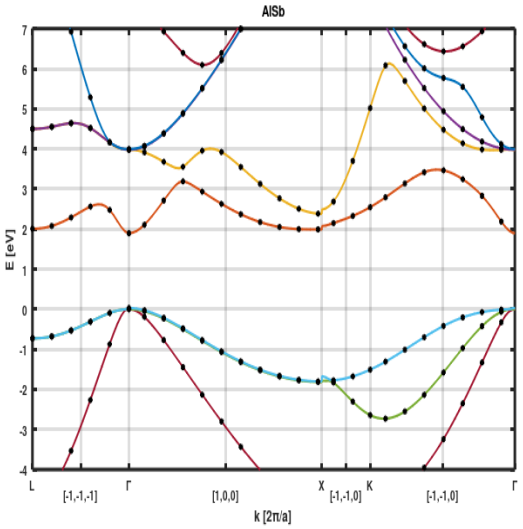

Fig. 12: Reproduced Band Structure of AlSb

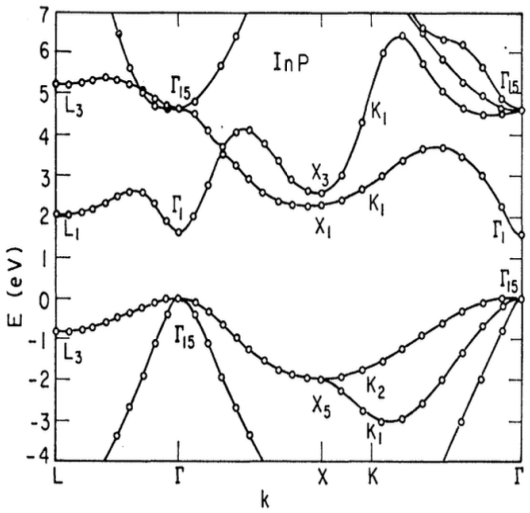

Fig. 13: Band Structure of InP. Cohen,Bergstresser.

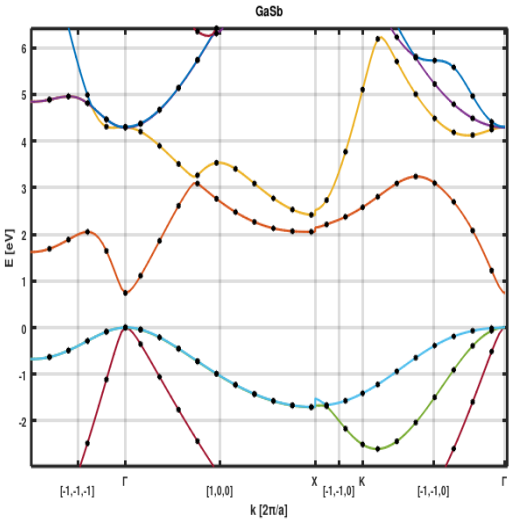

Fig. 16: Reproduced Band Structure of GaSb

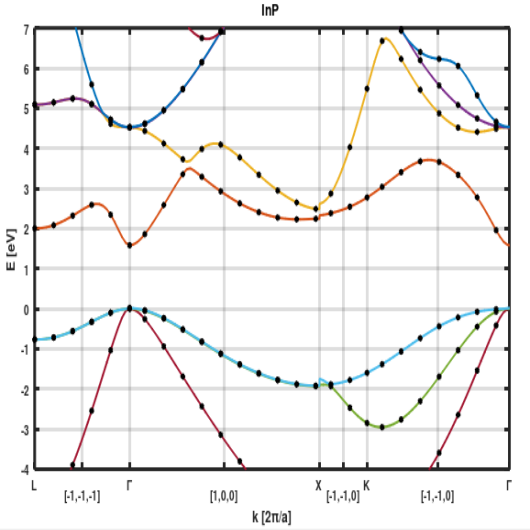

Fig. 14: Reproduced Band Structure of InP

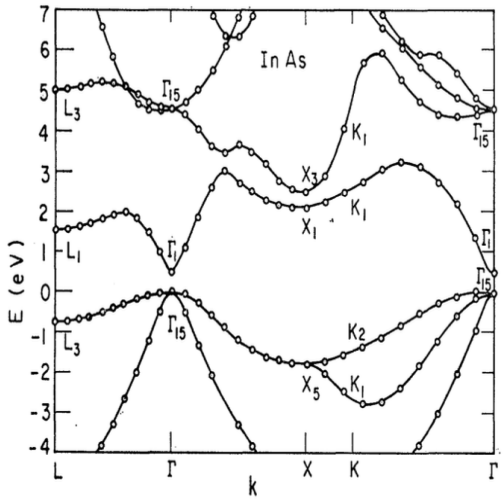

Fig. 17: Band Structure of InAs. Cohen,Bergstresser.

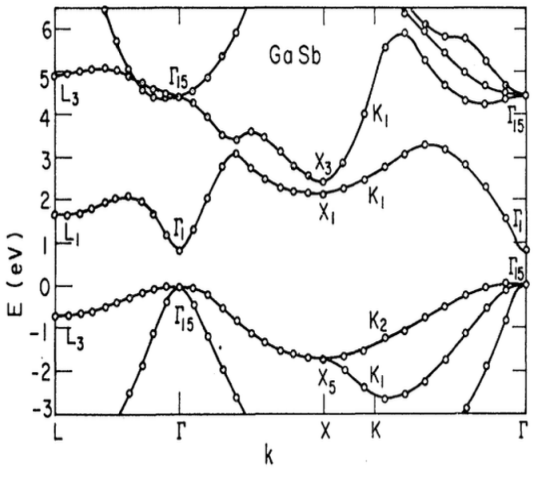

Fig. 15: Band Structure of GaSb. Cohen,Bergstresser.

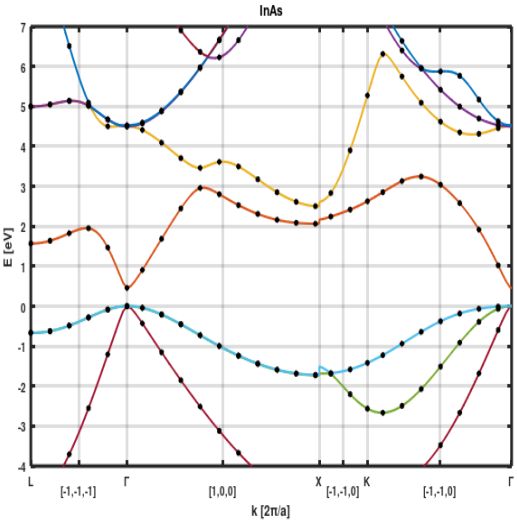

Fig. 18: Reproduced Band Structure of InAs

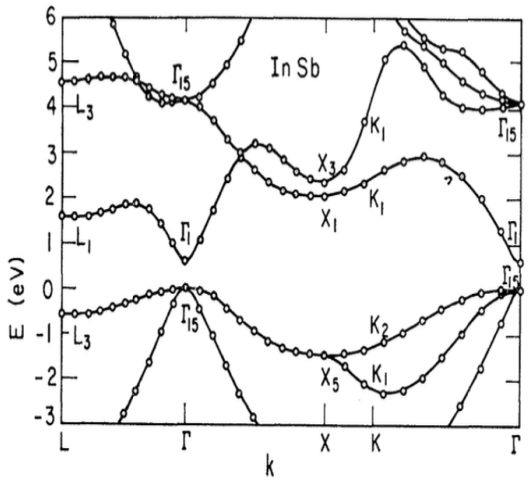

Fig. 19: Band Structure of InSb. Cohen,Bergstresser.

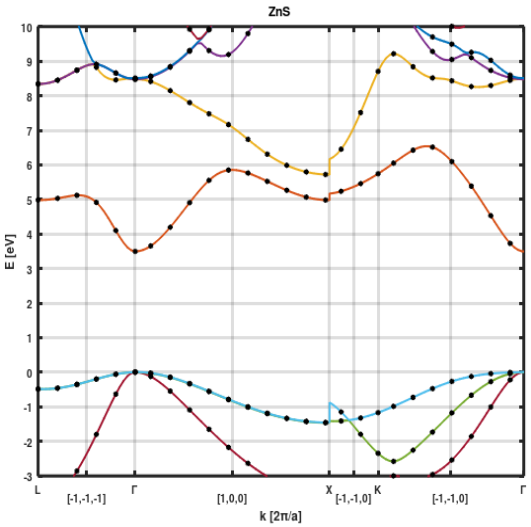

Fig. 22: Reproduced Band Structure of ZnS

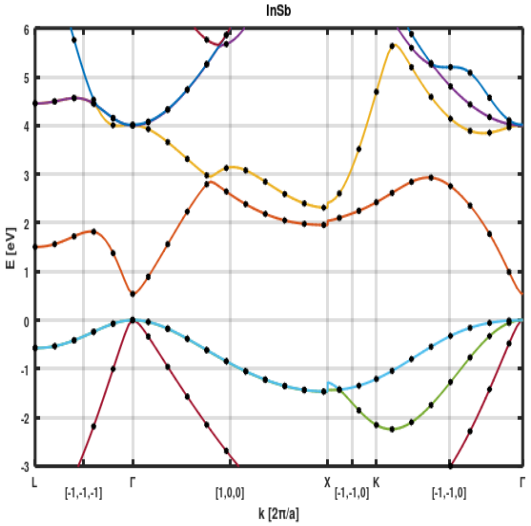

Fig. 20: Reproduced Band Structure of InSb

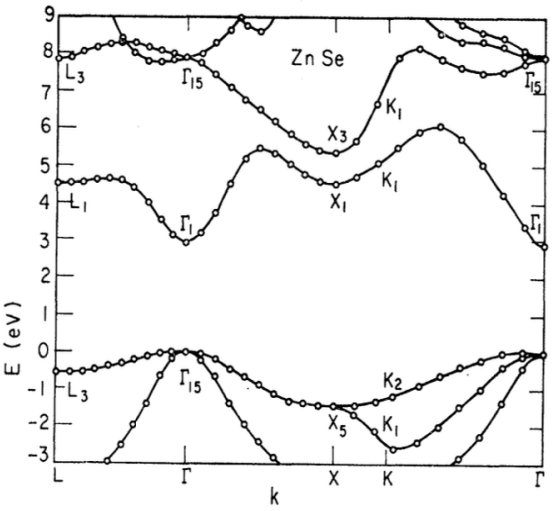

Fig. 23: Band Structure of ZnSe. Cohen,Bergstresser.

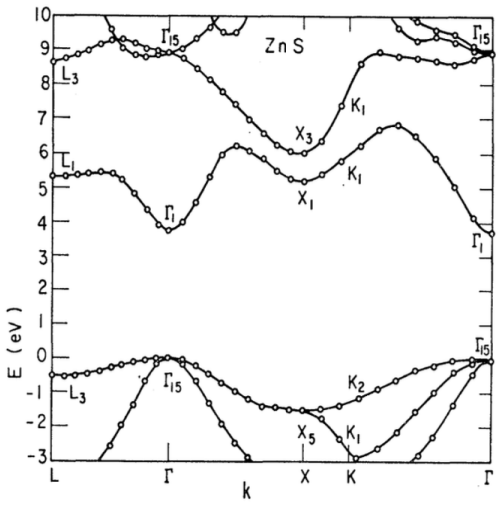

Fig. 21: Band Structure of ZnS. Cohen,Bergstresser.

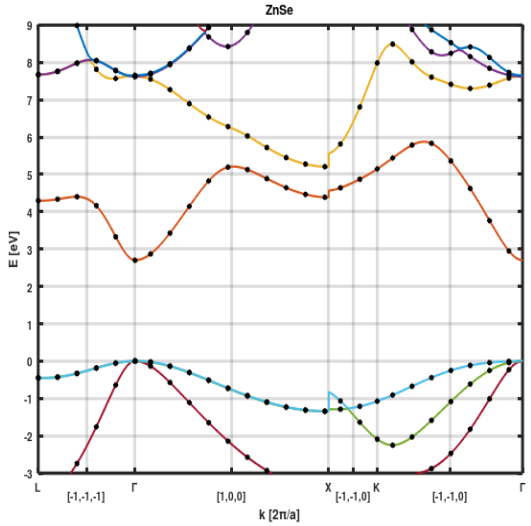

Fig. 24: Reproduced Band Structure of ZnSe

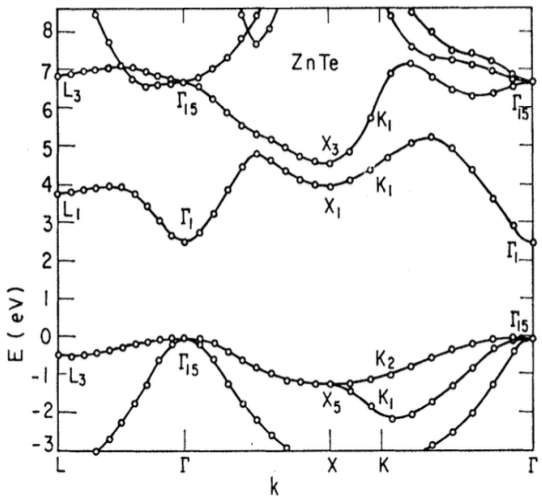

Fig. 25: Band Structure of ZnTe. Cohen,Bergstresser.

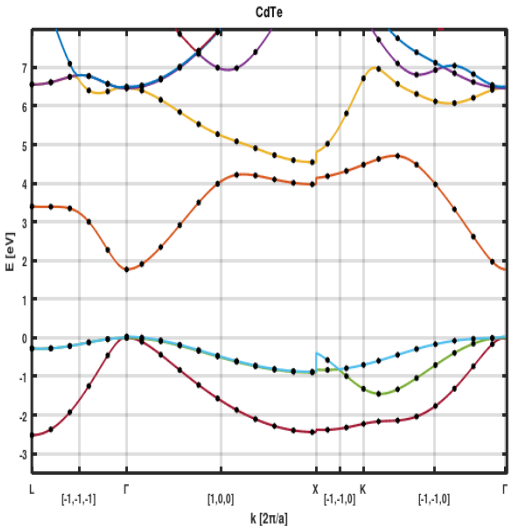

Fig. 28: Reproduced Band Structure of CdTe

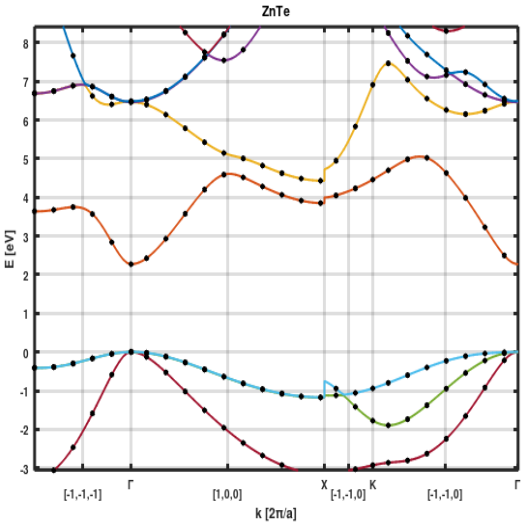

Fig. 26: Reproduced Band Structure of ZnTe

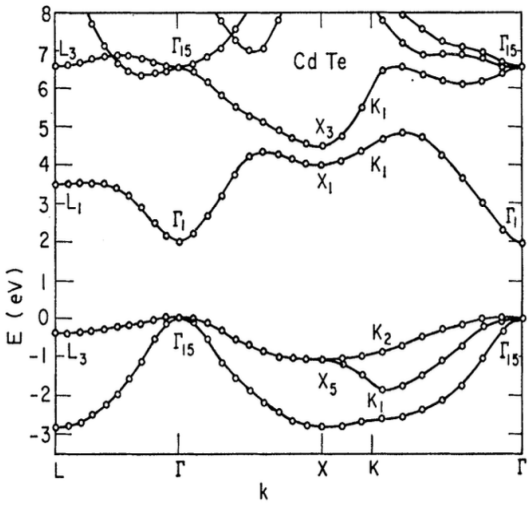

Fig. 27: Band Structure of CdTe. Cohen,Bergstresser.

energy level splitting, with differences ranging from 0.1 eV to 0.3 eV. Despite these minor variations, the overall trend aligns well with the seminal work, reinforcing the reliability of the computational approach. These differences may also stem from limitations in the original pseudoformfactor table, which provides data with only two significant digits.

Adjusting the valence band level: As informed in previous section, $V_{G=0}$ term should be taken care in order that the zero of the energy scale is set to the top of the valence band. Computationally, this requires a preliminary analysis of the results at the points obtained by a first run using $V_{G=0} = 0$. The top of the valence band comprises of the third energy band computed from the Hamiltonian matrix. Thus during the first run with $V_{G=0} = 0$, the X = max(bandstrucure(3,:))/Rydberg is calculated and in the subsequent run $V_{G=0}$ is set to '-X'. This sets the top of the valence band to the zero of the energy level. This is repeated for all the semiconductors and then the above figures were obtained.

IV. Conclusion

This project has successfully reproduced the electronic band structures of 14 semiconductors revealing reveals substantial alignment with Cohen and Bergstresser's work[1]. All the above presented result has been obtained from the computational work done using the Octave programming language, which can be found here *https://github.com/Akash22/band_structures*. To enhance precision in band structure calculations for these semiconductors, it is recommended to employ improved computational techniques. Such advancements hold the promise of delivering more accurate representations of semiconductor band structures, thereby contributing to a deeper understanding of their electronic properties.

This study successfully reproduced the The comprehensive comparison, depicted in Figures 1 to 14,

demonstrates a consistent match across all materials. The accuracy of the replicated outcomes affirms the reliability of the computational approach and contributes to the understanding of electron behaviour in crystals.

REFERENCES

[1] Marvin L Cohen and TK Bergstresser. Band structures and pseudopotential form factors for fourteen semiconductors of the diamond and zinc-blende structures. *Physical Review*, 141(2):789, 1966.

V. APPENDIX

TABLE I: Form factors in Rydberg units for 14 semiconductors

Material	V_0	VS_3	VS_8	VS_{11}	VA_3	VA_4	VA_{11}
Si	-0.7724	-0.21	0.04	0.08	0.00	0.00	0.00
Ge	-0.6951	-0.23	0.01	0.06	0.00	0.00	0.00
Sn	-0.5015	-0.20	0.00	0.04	0.00	0.00	0.00
GaP	-0.6775	-0.22	0.03	0.07	0.12	0.07	0.02
GaAs	-0.6527	-0.23	0.01	0.06	0.07	0.05	0.01
AlSb	-0.5107	-0.21	0.02	0.06	0.06	0.04	0.02
InP	-0.5627	-0.23	0.01	0.06	0.07	0.05	0.01
GaSb	-0.5112	-0.22	0.00	0.05	0.06	0.05	0.01
InAs	-0.5251	-0.22	0.00	0.05	0.08	0.05	0.03
InSb	-0.4460	-0.20	0.00	0.04	0.06	0.05	0.01
ZnS	-0.4677	-0.22	0.03	0.07	0.24	0.14	0.04
ZnSe	-0.4496	-0.23	0.01	0.06	0.18	0.12	0.03
ZnTe	-0.3925	-0.22	0.00	0.05	0.13	0.10	0.01
CdTe	-0.3117	-0.20	0.00	0.04	0.15	0.09	0.04